## 4. Conclusion

It is very complicated to calculate the second-order aberrations of complex analyser systems and mistakes are liable to be made.

Even if the matrix method is used the tediousness of the calculation is not altered.

The usefulness of the matrix representation comes from the fact that the over-all transfer matrix of the total system is easily written as a product of the transfer matrices of various parts of the system.

Hence the calculation of the second-order aberration is reduced to the mere mechanical calculation of matrix products.

For the case of the numerical calculation by digital computer, the matrix method may be advantageous to programming.

*Acknowledgement*

The author wishes to thank Professor H. MATSUDA for many helpful suggestions and discussions.

The author would also like to take this opportunity to express his thanks to Dr. S. KISAKA, Manager of the Laboratory, for his support and to Mr. K. SUGIHARA and Dr. C. OKAZAKI for their kind inspection of manuscript and their encouragement.

# Mattauch-Herzog Type Mass Spectrograph with a Two Stage Electrostatic Field

ISAO TAKESHITA

Research Laboratory, Wireless Division, Matsushita Electric Industrial Co., Kadoma, Osaka, Japan

(Z. Naturforschg. **21 a**, 14—25 [1966]; received 24 April 1965)

*Dedicated to Prof.* J. MATTAUCH *on his 70th birthday*

The most important advantage of the MATTAUCH–HERZOG type mass spectrograph is double focusing for all masses. One disadvantage, however, is the fact that the energy slit cannot control the velocity spread ($\beta$) independently of beam divergence ($\alpha$). This disadvantage is removed by substituting a two-stage electrostatic field for the usual single one.

General formulae for determining the distances between the elements of the optical system are derived.

Combinations of two cylindrical electrostatic fields with equal radii are chosen as a practical example. The condition to be fulfilled for a physically significant solution and the resolving power of this system are discussed.

The study of the second-order aberrations shows that $\alpha^2$ focusing for all masses can be achieved under suitable conditions. In addition, $\alpha\,\beta$ and $\beta^2$ aberrations can be made to vanish simultaneously at a point on the focal plane.

The design parameters are numerically computed and tabulated for several favorable examples. The total image defect is calculated for a typical example, and found to be very small for a wide range of masses.

Recently increasing interest has been shown in the potentiality of spark source mass spectrometry for the chemical analysis of solids.

An ion beam produced by a spark source, however, has a wide energy spread. Therefore, a double focusing mass spectrometer is required. In addition the intensity of an ion beam emerging from a spark source fluctuates rapidly and the spark produces considerable RF noise, so that electrical detection is prevented and photographic recording is inevitable.

A MATTAUCH–HERZOG type mass spectrograph [1] is especially well suited for this purpose, because it shows double focusing for all masses along a straight line.

One disadvantage of this type of instrument, however, is the fact that the energy slit cannot control the energy spread independently of beam divergence. Therefore, even if the energy slit is narrowed to infinitesimal width, the ion beam which enters the magnetic field still has a wide energy spread.

The author noticed that by substituting a combination of two electrostatic deflection fields for a single one in the usual MATTAUCH–HERZOG type mass spectrograph, the disadvantage mentioned above could be removed by setting an energy slit between the two electrostatic fields [1a].

[1] J. MATTAUCH and R. HERZOG, Z. Phys. **89**, 786 [1934].

[1a] I. TAKESHITA, Z. Naturforschg. **20 a**, 624 [1965].

HINTENBERGER and KÖNIG [2–5] investigated the image defects due to the second-order aberration of a MATTAUCH–HERZOG type mass spectrograph which consists of a cylindrical electrostatic field followed by a homogeneous magnetic field.

They proposed a number of favourable mass spectrographs with second-order double focusing on one point of the image line [6] or with very small aberration coefficients in a wide mass range [7].

The disadvantage of the slit system was still not removed and the image defects could possibly become unexpectedly large.

As this type of instrument is specified by the double focusing property for all masses, the correction of image defects for all masses is the important problem.

In the present work the correction of the second-order angular aberration for all masses will be discussed.

In this case, even when the coefficients of $\beta$-dependent second-order aberration are not zero, the image defects due to the coefficients can be controlled by the energy slit. Therefore, the correction of the second-order angular aberration for all masses is worth discussing.

For the numerical calculation the MADIC-II A in the author's laboratory is used.

## 1. First-Order Focusing

In the present work the matrix representation is employed for studying the ion trajectory [8].

A vector space is chosen whose components are $x$ (distance from optical axis), $\alpha$ (angle between ion trajectory and optical axis) and $\beta$ (relative velocity deviation). Then the field is expressed by a three-dimensional transfer matrix, and the overall transfer matrix of the multielement optical system is given by multiplication of the transfer matrices of various parts of the system.

Therefore, the optical system of a usual MATTAUCH–HERZOG type mass spectrograph is expressed as follows:

$$[T] = [l_4]\,[B]\,[d]\,[A]\,[l_1]\,, \tag{1.1}$$

where $[A]$ and $[B]$ are the transfer matrices of the electrostatic and magnetic field, respectively and $[l_1]$, $[d]$ and $[l_4]$ are the transfer matrices of field free regions whose lengthes are $l_1$, $d$, and $l_4$.

Then the MATTAUCH–HERZOG conditions [9] are governed by the following equations:

$$\begin{vmatrix} B_{11} & B_{13} \\ B_{21} & B_{23} \end{vmatrix} + A_{23} = 0\,, \tag{1.2}$$

$$A_{21}\,l_1 + A_{22} = 0\,, \tag{1.3}$$

$$B_{21}\,l_4 + B_{11} = 0\,, \tag{1.4}$$

where $A_{ij}$ and $B_{ij}$ are the matrix elements of $[A]$ and $[B]$.

As these equations are derived in a general way, it is not necessary to restrict $[A]$ to a single electrostatic field.

Here we assume $[A]$ to be a combination of two electrostatic fields $[E]$ and $[F]$ in tandem with a field free region between them.

The length of the field free region is $l_2 + l_3$, where $l_2$ is the distance from the first electrostatic field $[E]$ to the image point of the ion source by this field and $l_3$ is the distance between this image point and the second electrostatic field $[F]$.

Then the following matrix equation holds:

$$[A] = [F]\,[l_3]\,[l_2]\,[E]\,, \tag{1.5}$$

where $[l_2]$ and $[l_3]$ are the transfer matrices through the field free regions of length $l_2$ and $l_3$ respectively.

Substituting $A_{ij}$ from Eq. (1.5) in Eqs. (1.2) and (1.3) and considering that the following relation holds for $l_1$ and $l_2$:

$$E_{11}\,l_1 + E_{12} + (E_{21}\,l_1 + E_{22})\,l_2 = 0\,, \tag{1.6}$$

we obtain the following equations:

$$F_{21}\,l_3 + F_{22} = 0\,, \tag{1.7}$$

$$\begin{vmatrix} B_{11} & B_{13} \\ B_{21} & B_{23} \end{vmatrix} + F_{21}(E_{13} + E_{23}\,l_2) + F_{23} = 0\,. \tag{1.8}$$

From these equations $l_2$ and $l_3$ can be calculated, and substituting $l_2$ from Eq. (1.8) back in Eq. (1.6) we can calculate $l_1$.

In order to get a physically significant configuration, $l_1$, $l_2$, $l_3$, and $l_4$ should be positive.

[2] H. HINTENBERGER, H. WENDE, and L. A. KÖNIG, Z. Naturforschg. **10 a**, 605 [1955].
[3] H. HINTENBERGER and L. A. KÖNIG, Z. Naturforschg. **12 a**, 140 [1957].
[4] L. A. KÖNIG and H. HINTENBERGER, Z. Naturforschg. **12 a**, 377 [1957].
[5] H. HINTENBERGER and L. A. KÖNIG, Z. Naturforschg. **12 a**, 773 [1957].
[6] L. A. KÖNIG and H. HINTENBERGER, Nucl. Instr. **3**, 133 [1958].
[7] H. HINTENBERGER and L. A. KÖNIG, Nucl. Instr. **3**, 250 [1958].
[8] S. PENNER, Rev. Sci. Instr. **32**, 150 [1961].
[9] I. TAKESHITA, Mass Spectroscopy (Japan) **11**, 25 [1963].

The magnetic field $[B]$ used for the MATTAUCH–HERZOG type mass spectrograph should be homogeneous and satisfy the following geometrical relation

$$\vartheta'' = \frac{\varphi_m}{2} - \frac{\pi}{2}, \tag{1.9}$$

because the ion trajectories in the magnetic field should be like figures for all masses.

The meaning of the quantities $\vartheta''$, $\varphi_m$ etc. is illustrated in Fig. 1.

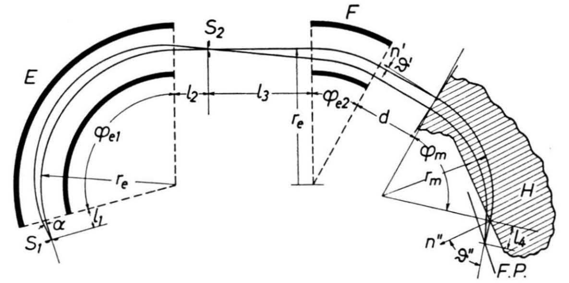


Fig. 1. Geometry and notations of MATTAUCH–HERZOG type mass spectrograph with two-stage electrostatic field. $S_1$: Source slit, $S_2$: Energy slit, E, F: Electrostatic field, H: Magnetic field, F.P.: Focal plane.

The parameters of the magnetic field have an effect on $l_1$ and $l_2$ through $B_{11} B_{23} - B_{21} B_{13}$, so that for a given $B_{11} B_{23} - B_{21} B_{13}$ the effect of the magnets on the configuration of the electric fields is the same, even though the geometry of the magnetic field is different.

In this paper $D_3$ is defined by:

$$D_3 \equiv B_{11} B_{23} - B_{21} B_{13}.$$

In the second-order approximation, this constant is also very important and it is of some interest to examine its value.

Using the matrix elements of a homogeneous magnetic field with linear field boundaries, and considering Eq. (1.9) we obtain

$$D_3 = \pm \{\sin \varphi_m + (1 - \cos \varphi_m) \tan \vartheta'\}. \tag{1.10}$$

The upper sign is valid if the deflections in the magnetic field and the first electric field are in the same direction, and the lower sign, for deflections in opposite directions.

The position of double focusing point with respect to the magnetic field is given by

$$\frac{l_4}{r_m} = \frac{\pm D_3 - \tan \frac{1}{2} \varphi_m}{\pm D_3} \sin \varphi_m. \tag{1.11}$$

Fig. 2 gives the results of the calculations of $D_3$ for various values of $\vartheta'$ and the shaded area in Fig. 2 shows the region for negative $l_4$.

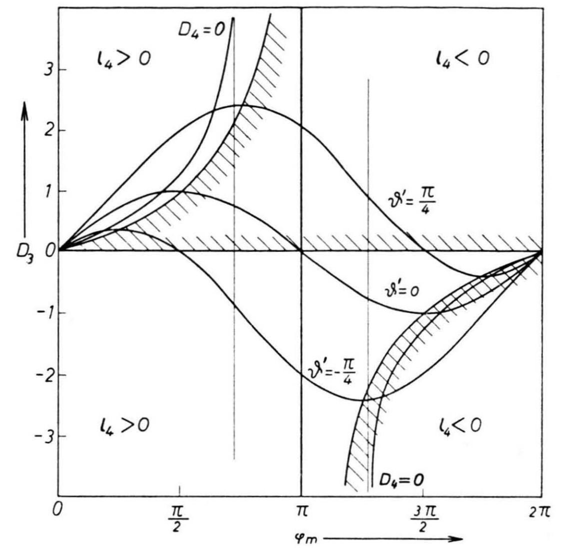


Fig. 2. Plots of $D_3$ vs. $\varphi_m$ for three values of the incident angle $\vartheta'$. The shaded area represents the region where $l_4 < 0$.

For a practical example, let $[E]$ and $[F]$ be two cylindrical electrostatic fields in an equal radius $(r_e)$ of center beam, whose deflection angles are $\varphi_{e1}$ and $\varphi_{e2}$, respectively. For simplicity the following abbreviations are used:

$$\sqrt{2}\, \varphi_{e1} = \varphi_1,$$
$$\sqrt{2}\, \varphi_{e2} = \varphi_2. \tag{1.12}$$

Substituting the matrix elements of these fields in Eqs. (1.7) and (1.8) we obtain

$$\frac{l_3}{r_e} = \frac{1}{\sqrt{2}} \cot \varphi_2, \tag{1.13}$$

$$\frac{l_2}{r_e} = \frac{1}{\sin \varphi_1 \sin \varphi_2} \left\{ \frac{D_3}{2} - \frac{\sin \varphi_2}{\sqrt{2}} (1 \mp 1 - \cos \varphi_1) \right\}. \tag{1.14}$$

Substitution of Eq. (1.14) in Eq. (1.6) gives

$$\frac{l_1}{r_e} = \frac{\frac{1}{\sqrt{2}} D_3 \cos \varphi_1 + \{1 - (1 \mp 1) \cos \varphi_1\} \sin \varphi_2}{\{D_3 - (1 \mp 1) \sqrt{2} \sin \varphi_2\} \sin \varphi_1}. \tag{1.15}$$

The upper sign is valid if the deflections in the two electrostatic fields are in the same direction and the lower sign, for deflections in opposite directions.

The area where $l_1$, $l_2$, $l_3$ are all positive may be mapped on the $\varphi_1 - \varphi_2$ plane for various $D_3$. Several typical diagrams are given in Fig. 3 a, b, c, and

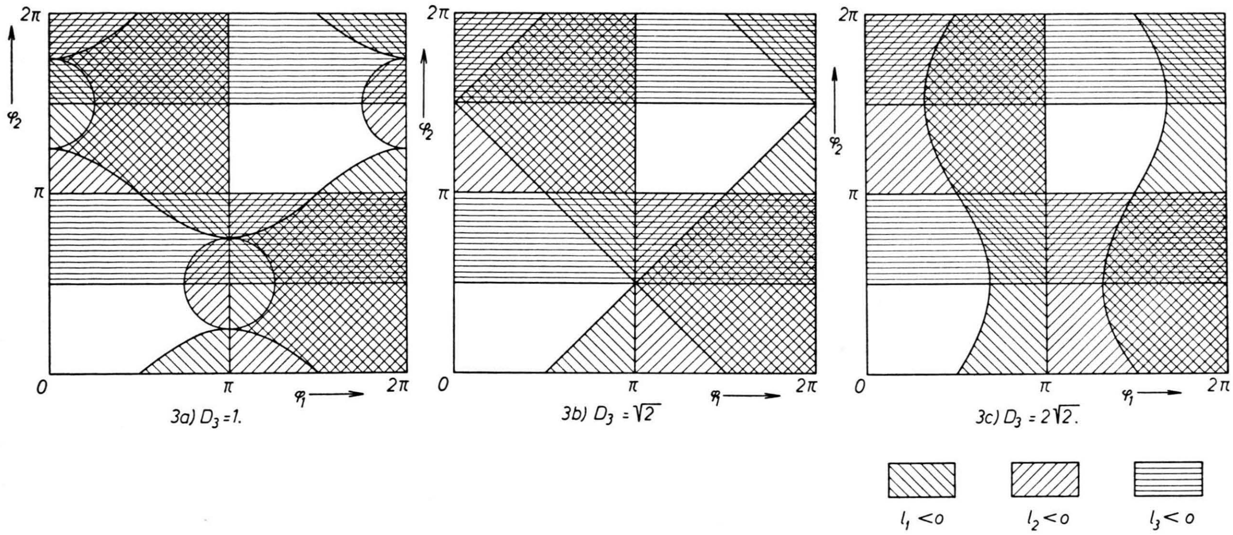


Fig. 3. Region of the physically significant configuration for three values of $D_3$. Deflection in the two electrostatic fields in the same direction. Unshaded area shows the region.

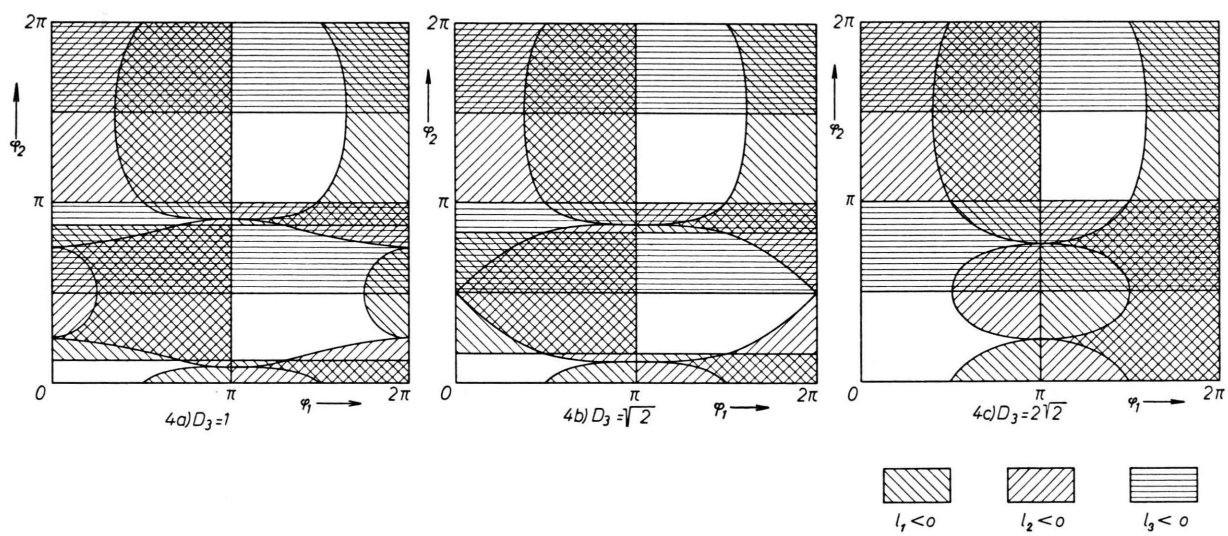


Fig. 4. Region of the physically significant configuration for three values of $D_3$. Deflection in the two electrostatic fields in the opposite direction. Unshaded area shows the region.

Fig. 4 a, b, c. The available field are the field combinations represented by the points lying within the unshaded area in these figures.

The resolving power ($R$) of a MATTAUCH–HERZOG type mass spectrograph is written generally in the following form:

$$R = \frac{1}{2\,s}\left|\frac{A_{23}}{A_{21}}\right|. \tag{1.16}$$

where $s$ is the width of the source slit.

Substitution of the matrix elements from Eq. (1.5) gives the analytical expression of resolving power for the present case, but using the matrix element $G_{ij}$ described by

$$[l_2]\,[E] = [G]\,, \tag{1.17}$$

we have

$$R = \frac{r_e}{s\,k^2}\left|\frac{1}{G_{11}} - 1 \mp \frac{1}{G_{11}}\right|, \tag{1.18}$$

where $k$ is a constant characterizing the field, such as $k = \sqrt{2}$ for a cylindrical electrostatic field. The upper sign is for deflections in the same direction and the lower sign, for deflections in the opposite direction. In the former case the resolving power is the same as that of the usual MATTAUCH–HERZOG type instrument.

In the latter case the resolving power is given by

$$R = \frac{r_e}{2s} \left| \frac{D_3}{2\sqrt{2}\sin\varphi_2 - D_3} \right| . \tag{1.19}$$

This implies the possibility of increasing the resolving power.

## 2. Second-Order Aberration

### *a) General expressions of second-order aberration*

An extensive study of the second-order aberrations of a MATTAUCH–HERZOG type mass spectrograph was made by HINTENBERGER and KÖNIG[3–5].

Following their method we could calculate the second-order aberrations of the present system which consists of a two-stage electrostatic field and a homogeneous magnetic field in tandem.

The matrix method, however, seems more convenient[10]. The ion trajectory in the field which is homogeneous in the direction perpendicular to the plane on which the optical axis lies is conveniently described by a nine-dimensional transfer matrix, if we choose the vector space as follows:

$$(x, \alpha, \beta, x^2, x\alpha, \alpha^2, x\beta, \alpha\beta, \beta^2). \tag{2.1}$$

The matrix elements $A_{ij}$ of a cylindrical electrostatic field or a homogeneous magnetic field are related to HINTENBERGER's notation[3]:

$$\begin{array}{llll}
A_{11} = \varkappa_{1b}, & (\mu_{1b}), & A_{21} = \lambda_{1b}/r_e, & (\nu_{1b}/r_m), \\
A_{12} = r_e\,\varkappa_{1a}, & (r_m\,\mu_{1a}), & A_{22} = \lambda_{1a}, & (\nu_{1a}), \\
A_{13} = r_e\,\varkappa_{2a}, & (r_m\,\mu_{2a}), & A_{23} = \lambda_{2a}, & (\nu_{2a}), \\
A_{14} = \varkappa_{11c}/r_e, & (\mu_{11c}/r_m), & A_{24} = \lambda_{11c}/r_e^2, & (\nu_{11c}/r_m^2), \\
A_{15} = \varkappa_{11b}, & (\mu_{11b}), & A_{25} = \lambda_{11b}/r_e, & (\nu_{11b}/r_m), \\
A_{16} = r_e\,\varkappa_{11a}, & (r_m\,\mu_{11a}), & A_{26} = \lambda_{11a}, & (\nu_{11a}), \\
A_{17} = \varkappa_{12b}, & (\mu_{12b}), & A_{27} = \lambda_{12b}/r_e, & (\nu_{12b}/r_m), \\
A_{18} = r_e\,\varkappa_{12a}, & (r_m\,\mu_{12a}), & A_{28} = \lambda_{12a}, & (\nu_{12a}), \\
A_{19} = r_e\,\varkappa_{22a}, & (r_m\,\mu_{22a}), & A_{29} = \lambda_{22a}, & (\nu_{22a}).
\end{array} \tag{2.2}$$

Other matrix elements are expressed by these $A_{1j}$ and $A_{2j}$.

Thus the matrix method can be extended to include the second-order terms. Eqs. (1.1) or (1.5) may be considered the matrix equation of these nine-dimensional transfer matrices, and the first-order theory is included in these equations.

[10] I. TAKESHITA, Z. Naturforschg. **20 a**, 9 [1965].

The ordinate $x$ of an ion beam on the plane vertical to the optical axis at the first-order double focusing point is expressed by

$$x = T_{16}\,\alpha^2 + T_{18}\,\alpha\beta + T_{19}\,\beta^2, \tag{2.3}$$

provided the width of source slit is infinitely narrow. These terms are the second-order image defects.

Using Eq. (1.1) and considering Eqs. (1.2), (1.3), and (1.4), we obtain the following expressions:

$$T_{16} = -\frac{r_e^2\,r_m}{a_{21}^2\,b_{21}} \left\{ \frac{D_4}{r_m^2} + (a_{24}\,a_{22}^2 - a_{25}\,a_{21}\,a_{22} + a_{26}\,a_{21}^2)\frac{1}{r_e^2} \right\}, \tag{2.4}$$

$$T_{18} = \frac{r_e\,r_m}{a_{21}\,b_{21}} \left\{ -\begin{vmatrix} a_{21} & a_{27} \\ a_{22} & a_{28} \end{vmatrix} \frac{1}{r_e} + 2\,D_4 \left(a_{13} - \frac{d}{r_e} D_3\right)\frac{r_e}{r_m^2} + (D_7 - D_3\,D_5)\frac{1}{r_m} \right\}, \tag{2.5}$$

$$T_{19} = -\frac{r_m}{b_{21}} \left\{ a_{29} + D_4 \left(a_{13} - \frac{d}{r_e} D_3\right)^2 \frac{r_e^2}{r_m^2} + (D_7 - D_3\,D_5)\left(a_{13} - \frac{d}{r_e} D_3\right)\frac{r_e}{r_m} + D_3^2 D_6 - D_3\,D_8 + D_9 \right\}, \tag{2.6}$$

where we have introduced the abbreviation

$$D_j = \begin{vmatrix} b_{11} & b_{1j} \\ b_{21} & b_{2j} \end{vmatrix}, \tag{2.7}$$

$a_{ij}$ and $b_{ij}$ being the dimensionless factors of $A_{ij}$ and $B_{ij}$.

### *b) Mass spectrograph with second-order direction focusing for all masses*

In order to make the coefficient of the second-order angular aberration be zero for all masses, the optical system must fulfill the following conditions

$$D_4 = 0, \tag{2.8}$$

$$a_{24}\,a_{22}^2 - a_{25}\,a_{21}\,a_{22} + a_{26}\,a_{21}^2 = 0. \tag{2.9}$$

If the deflections in the magnetic field and the first electrostatic field are in the same direction, then the first condition is fulfilled when the geometry of the magnetic field satisfies the following relation:

$$\tan\vartheta' = \frac{2\cos\frac{1}{2}\varphi_m(\cos^2\frac{1}{2}\varphi_m - 2\sin^2\frac{1}{2}\varphi_m)}{(1 - 6\cos^2\frac{1}{2}\varphi_m)\sin\frac{1}{2}\varphi_m}. \tag{2.10}$$

In this case $D_3$ and $l_4$ are given as follows:

$$D_3 = \frac{3\sin\varphi_m}{6\cos^2\frac{1}{2}\varphi_m - 1}, \tag{2.11}$$

$$\frac{l_4}{r_m} = \frac{1}{3}\tan\frac{\varphi_m}{2}. \tag{2.12}$$

As $l_4$ must be positive, the deflection angle $\varphi_m$ must be within $[0, \pi]$.

Plots of $D_3$, $\vartheta'$, $\vartheta''$, $l_4$ etc. as a function of $\varphi_m$ are given in Fig. 5.

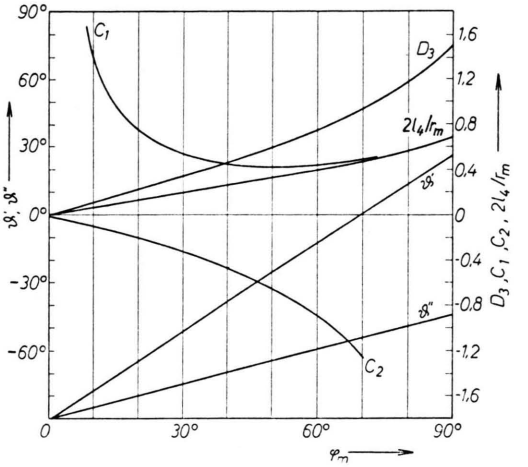


Fig. 5. Calculated curves for various constants of the magnetic field satisfying $D_4=0$ as a function of $\varphi_m$.

Provided the field $[A]$ consists of only one cylindrical electrostatic field, then the left side of Eq. (2.9) does not vanish under the condition (1.2). In the present case one may possibly find the solutions which satisfy this condition.

The physical meaning of Eq. (2.9) is that the ion beam entering the magnetic field is parallel in second-order approximation.

Since the combinations of two electrostatic fields in the same sense intuitively seem favourable for aberrations, the following study is confined to this case. Then Eq. (2.9) becomes

$$\frac{\sqrt{2}}{\sin^2\varphi_1}\left[\left(\frac{\sqrt{2}}{24}D_3^3+\frac{3}{2}\sin\varphi_2\right)X^2+\left(\frac{3\sqrt{2}}{2}D_3\sin^2\varphi_2 + \frac{3}{2}D_3^2\sin\varphi_2\right)X+\left(\frac{3}{2}\sin^3\varphi_2-\frac{3}{2}\sin\varphi_2 + \frac{3\sqrt{2}}{4}D_3\sin^2\varphi_2+\frac{3}{4}D_3^2\sin\varphi_2+\frac{\sqrt{2}}{3}D_3^3\right)\right]=0\,. \tag{2.13}$$

where $X=\cos\varphi_1$.

As the equation in the square bracket is a quadratic equation of $X$, the solution is easily derived in an analytic form. As $X$ is a trigonometrical function of $\varphi_1$, $X$ should be real and within $[-1, 1]$. The area where the roots of the quadratic equation are real is mapped in Fig. 6.

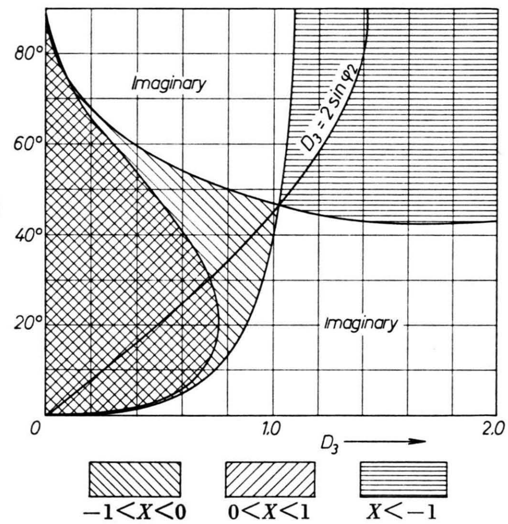


Fig. 6. Region of real roots of Eq. (2.13).

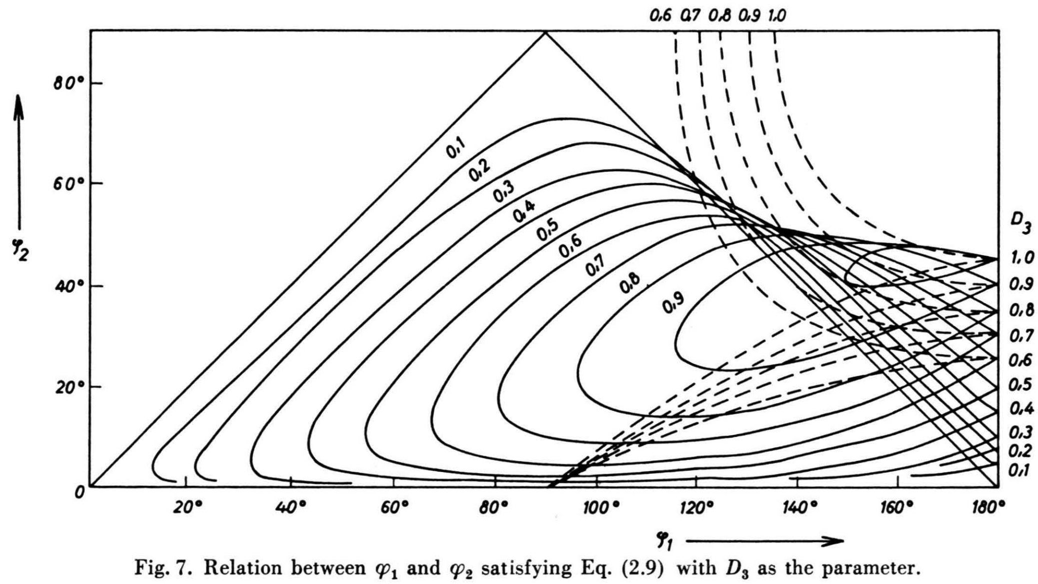


Fig. 7. Relation between $\varphi_1$ and $\varphi_2$ satisfying Eq. (2.9) with $D_3$ as the parameter.

At the critical point, $(D_3=6/\sqrt{34},\ \varphi_2=\sin^{-1} 13/\sqrt{17})$, $\varphi_1$ is equal to $\pi$ and $1/\sin^2\varphi_1$ diverges, but the limiting value of the left side of Eq. (2.13) is still zero. If $D_3$ is smaller than $6/\sqrt{34}$, the solution satisfying Eq. (2.13) corresponds to a closed curve on the $\varphi_1-\varphi_2$ plane.

This curve contracts with increasing $D_3$ and reduces to a point on the line $\varphi_1=\pi$ when $D_3$ equals $6/\sqrt{34}$. For larger $D_3$ this curve vanishes. The solid lines in Fig. 7 show these curves.

It is clear that the field combinations corresponding to the coordinates $\varphi_1$, $\varphi_2$ on these curves for respective $D_3$ satisfy Eq. (2.9). Practical significance requires positive $l_1$, $l_2$ and $l_3$. Accordingly only the part of these curves which lie in the unshaded area of Fig. 4 for respective $D_3$ is practically significant. The dashed lines in Fig. 7 show the boundaries of these areas.

By taking a positive root in the analytical solution of $X$, positive $l_1$ and $l_2$ are always assured though the analytical proof is difficult. Therefore, the following discussion is restricted to solutions with positive roots. Figs. 8 and 9 give the results of the numerical calculations of $l_1/r_e$ and $l_2/r_e$ for various $D_3$.

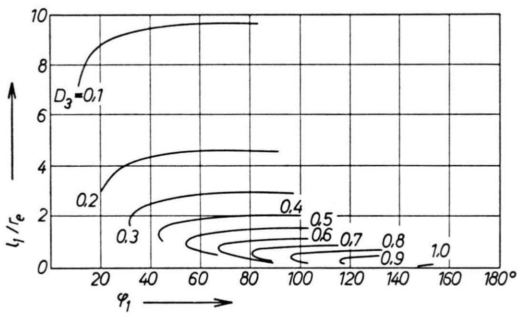


Fig. 8. Position of source with respect to the first electrostatic field as a function of $\varphi_1$ for various values of $D_3$.

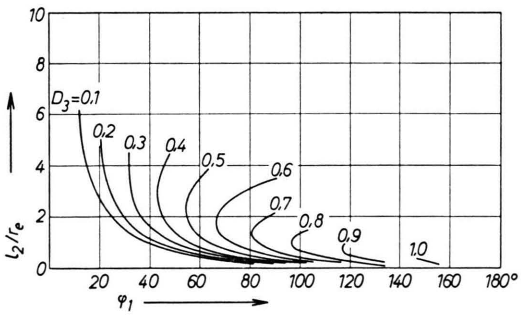


Fig. 9. Position of intermediate image with respect to the first electrostatic field as a function of $\varphi_1$ for various values of $D_3$.

*c) The correction of β-dependent image defects*

In the last section we knew that we could build mass spectrographs whose second-order angular aberrations are corrected for all masses. Putting $D_4=0$ in Eq. (2.5), we have the expression for the coefficients of $\alpha\beta$ aberrations of these remarkable mass spectrographs as follows:

$$T_{18}=\frac{r_e r_m}{a_{21} b_{21}}\left\{-\begin{vmatrix} a_{21} & a_{27} \\ a_{22} & a_{28}\end{vmatrix}\frac{1}{r_e}+(D_7-D_3 D_5)\frac{1}{r_m}\right\}. \tag{2.14}$$

The coefficient of $1/r_m$ is expressed as a function of $\varphi_m$:

$$C_1 \equiv D_7-D_3 D_5=\frac{3\cos\frac{1}{2}\varphi_m}{(6\cos^2\frac{1}{2}\varphi_m-1)^2 \sin\frac{1}{2}\varphi_m}, \tag{2.15}$$

and as easily proved $C_1$ is always positive when $\varphi_m$ is within $[0,\pi]$ (Fig. 5).

Therefore, it is impossible to make $T_{18}$ vanish independent of $r_m$. At one point on the photographic plate, however, this term may posibly be canceled by the first term. This condition is

$$r_{m0}/r_e=C_1/D_A, \tag{2.16}$$

where $D_A$ is the abbreviation of $a_{21}a_{28}-a_{22}a_{27}$ and $r_{m0}$ denotes the particular $r_m$ which satisfys this condition. To be physically significant, this ratio should be positive. In the present case, $D_A$ is expressed by the following equation:

$$\begin{aligned} D_A=\frac{\sqrt{2}}{3}\Big[&\sin\varphi_1(8+\cos^2\varphi_2)+\frac{4D_3}{\sqrt{2}} \\ &+\cos\varphi_2\left(\frac{5D_3}{\sqrt{2}}-3\sin\varphi_2\right) \\ &-\frac{1}{\sin\varphi_1}\Big\{(8+3\cos\varphi_1+\cos^2\varphi_1)\sin^2\varphi_2 \\ &+\frac{D_3}{\sqrt{2}}(11+13\cos\varphi_1)\sin\varphi_2 \\ &+2D_3^2(2\cos\varphi_1+1)\Big\}\Big]. \end{aligned} \tag{2.17}$$

The numerical evaluation of Eq. (2.7) proves that $D_A$ is always positive except for small $D_3$. Fig. 10 shows the lines of constant $r_{m0}/r_e$ on the $D_3-\varphi_2$ plane.

Considering $D_4=0$ and $D_9=0$, the coefficient of $\beta^2$ aberration becomes

$$T_{19}=-\frac{r_m}{b_{21}}\left\{a_{29}+(D_7-D_3 D_5)\left(a_{13}-\frac{d}{r_e}D_3\right)\frac{r_e}{r_m}+C_2\right\} \tag{2.18}$$

where $C_2=D_3^2 D_6-D_3 D_8$.

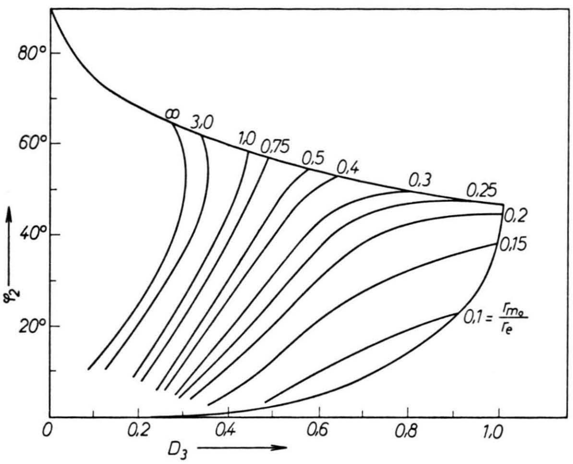


Fig. 10. Plot of constant $r_{m0}/r_e$ lines on $D_3-\varphi_2$ plane.

In order to correct $\alpha\beta$ and $\beta^2$ aberration at one point on the photographic plate, $r_m$ of Eq. (2.18) must be replaced by $r_{m0}$. Then Eq. (2.18) becomes

$$T_{19}\,|r_{m0} = -\frac{r_{m0}}{b_{21}}\left\{a_{29} + D_A\, a_{13} + C_2 - D_A\, D_3\, \frac{d}{r_e}\right\}. \tag{2.19}$$

The condition of vanishing $T_{19}$ is solved in terms of $d/r_e$ as follows:

$$\frac{d}{r_e} = \frac{a_{29} + D_A\, a_{13} + C_2}{D_A\, D_3}. \tag{2.20}$$

In the present case $C_2$ is given by the following equation

$$C_2 = -D_3{}^3\, \frac{1 + 3\cos^2 \frac{1}{2}\varphi_m}{6\sin^2 \frac{1}{2}\varphi_m}, \tag{2.21}$$

and plotted in Fig. 5.

$a_{13}$ and $a_{29}$ can be written as follows:

$$a_{13} = \frac{\sin\varphi_1}{\sin\varphi_2} + \frac{D_3}{\sqrt{2}}\cot\varphi_2 + 1, \tag{2.22}$$

$$\begin{aligned} a_{29} = \sqrt{2}\Big[\sin(\varphi_1+\varphi_2) &+ \frac{D_3}{\sqrt{2}}\left(\frac{7}{6} + \frac{4}{3}\cos\varphi_1\right) \\ &+ \frac{1}{\sin\varphi_2}\Big\{\frac{3}{2}\left(\sin^2\varphi_2 - \sin^2\varphi_1\right) \\ &- \frac{D_3}{\sqrt{2}}\left(\frac{4}{3} + \frac{5}{3}\cos\varphi_2\right)\sin\varphi_1 \\ &- D_3{}^2\left(\frac{1}{12} + \frac{2}{3}\cos\varphi_2\right)\Big\}\Big]. \end{aligned} \tag{2.23}$$

The constant $d/r_e$ lines satisfying Eq. (2.20) are plotted in Fig. 11. The results clearly suggest the possibility of an excellent mass spectrograph whose $\alpha\beta$ and $\beta^2$ aberrations are zero at one point on the photographic plate by a particular choice of $d/r_e$, in addition to achieving first- and second-order angular focusing and first-order velocity focusing for all masses.

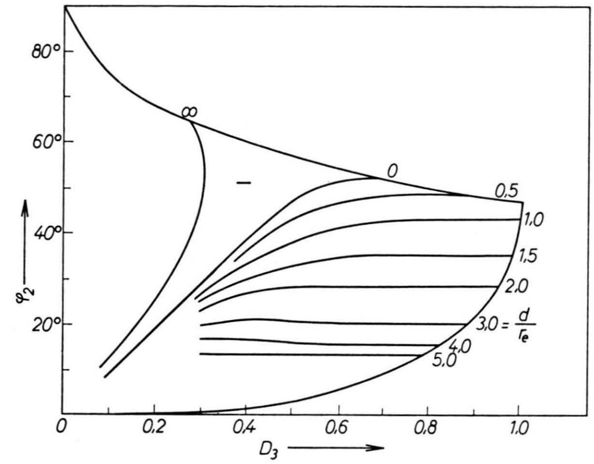


Fig. 11. Plot of constant $d/r_e$ lines on $D_3-\varphi_2$ plane.

The essential problem, however, is not to correct the image defects for one mass but to reduce them for a wide mass range. The change of the coefficients along the focal plane should be examined.

With $r_m/r_{m0} = \tau$, Eq. (2.14) yields the relative aberration coefficient $T_{18}/r_m$ as a function of $\tau$:

$$\frac{T_{18}}{r_m} = \frac{2\sin^2\frac{1}{2}\varphi_m}{D_3{}^2}\, D_A\left(1 - \frac{1}{\tau}\right). \tag{2.24}$$

Substituting Eq. (2.20) in Eq. (2.18), we obtain

$$\frac{T_{19}}{r_m} = \frac{2\sin^2\frac{1}{2}\varphi_m}{D_3}\,(a_{29} + C_2)\left(1 - \frac{1}{\tau}\right). \tag{2.25}$$

These are the same functions of $\tau$ and they converge for $\tau = \infty$.

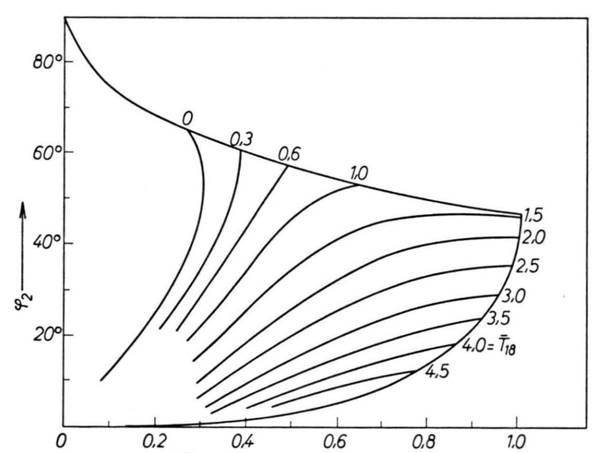


Fig. 12. Plot of constant $\overline{T}_{18}$ lines on $D_3-\varphi_2$ plane.

Let $\overline{T}_{18}$ and $\overline{T}_{19}$ be these limitting values, then

$$\overline{T}_{18} = \frac{2 \sin^2 \frac{1}{2} \varphi_{\mathrm{m}}}{D_3^2} D_{\mathrm{A}} , \tag{2.26}$$

$$\overline{T}_{19} = \frac{2 \sin^2 \frac{1}{2} \varphi_{\mathrm{m}}}{D_3} (a_{29} + C_2) . \tag{2.27}$$

Constant $\overline{T}_{18}$ lines and constant $\overline{T}_{19}$ lines plotted on the $D_3 - \varphi_2$ plane are given in Fig. 12 and in Fig. 13.

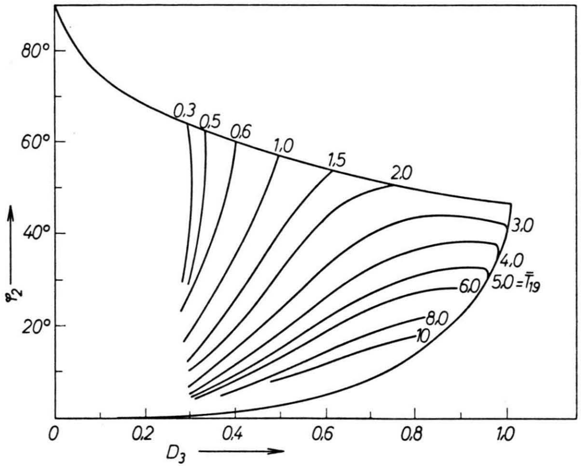


Fig. 13. Plot of constant $\overline{T}_{19}$ lines on $D_3 - \varphi_2$ plane.

### *d) Discussion*

By replacing of an electrostatic field in an usual Mattauch–Herzog type mass spectrograph by a combination of two electrostatic fields in tandem, a remarkable mass spectrograph can be designed.

The important advantages of these instruments are as follows:

1. The first-order double focusing for all masses is achieved.
2. A real image of the source slit exists between two electrostatic fields, and independent control of $\alpha$ and $\beta$ is possible.
3. The second-order angular aberration is corrected for all masses.
4. The simultaneous correction of $\alpha\beta$ and $\beta^2$ aberrations is achieved at one point on the photographic plate.

A numerous variety of mass spectrographs possessing these advantages are possible. From the practical point of view, a magnet of small deflection angle ($\varphi_{\mathrm{m}}$) or large incident angle ($\vartheta'$) is not favourable. This fact implies that $D_3$ should not be

| No | $D_3$ | $\varphi_{\mathrm{m}}$ | $\vartheta'$ | $\vartheta''$ | $\varphi_{\mathrm{e1}}$ | $\varphi_{\mathrm{e2}}$ | $l_1/r_{\mathrm{e}}$ | $l_2/r_{\mathrm{e}}$ | $l_3/r_{\mathrm{e}}$ | $l_4/r_{\mathrm{m}}$ | $r_{\mathrm{m0}}/r_{\mathrm{e}}$ | $d/r_{\mathrm{e}}$ | $\overline{T}_{18}$ | $\overline{T}_{19}$ |
|---|---|---|---|---|---|---|---|---|---|---|---|---|---|---|
| 1 | 1.029 | 74° 24′ | 5° 09′ | −52° 48′ | 127° 17′ | 33° 01′ | 0 | 0 | 0.666 | 0.253 | 0.272 | 0.473 | 1.274 | −1.571 |
| 2 | 1.00 | 73° 08′ | 3° 28′ | −53° 26′ | 112° 49′ | 33° | 0.186 | 0.0711 | 0.667 | 0.247 | 0.244 | 0.587 | 1.429 | −2.229 |
| 3 | 1.00 | 73° 08′ | 3° 28′ | −53° 26′ | 105° 40′ | 30° | 0.129 | 0.260 | 0.774 | 0.247 | 0.180 | 1.002 | 1.940 | −2.959 |
| 4 | 0.943 | 70° 32′ | 0 | −54° 44′ | 104° 34′ | 33° 30′ | 0.342 | 0.0787 | 0.772 | 0.236 | 0.252 | 0.527 | 1.402 | −2.432 |
| 5 | 0.943 | 70° 32′ | 0 | −54° 44′ | 95° 22′ | 30° | 0.306 | 0.282 | 0.774 | 0.236 | 0.183 | 0.997 | 1.931 | −3.349 |
| 6 | 0.9 | 68° 28′ | − 2° 44′ | −55° 46′ | 103° 43′ | 34° 18′ | 0.439 | 0.0180 | 0.626 | 0.227 | 0.291 | 0.312 | 1.230 | −2.230 |
| 7 | 0.9 | 68° 28′ | − 2° 44′ | −55° 46′ | 90° 06′ | 30° | 0.403 | 0.299 | 0.774 | 0.227 | 0.187 | 0.995 | 1.915 | −3.409 |
| 8 | 0.8 | 63° 16′ | − 9° 37′ | −58° 22′ | 94° 02′ | 35° 21′ | 0.650 | 0.0546 | 0.593 | 0.205 | 0.309 | 0.232 | 1.207 | −2.167 |
| 9 | 0.7 | 57° 28′ | −17° 12′ | −61° 16′ | 87° 54′ | 36° 46′ | 0.880 | 0.0549 | 0.553 | 0.183 | 0.370 | 0.009 | 1.069 | −1.827 |
| 10 | 0.6 | 51° 01′ | −25° 33′ | −64° 29′ | 74° 32′ | 36° | 1.147 | 0.206 | 0.575 | 0.159 | 0.403 | 0.090 | 1.063 | −1.616 |

Table 1. Examples of Mass Spectrographs with corrected $\alpha^2$ image defect for all masses and corrected $\beta$-dependent image defects at one point of the photoplate.

too small. On the other hand the achievement of $\alpha^2$-focusing requires $D_3$ smaller than $6/\sqrt{34}$. Fig. 5 shows that these conditions are compatible and magnets characterized by $D_3 \simeq 1$ are possibly useful. Especially, the vertical entry is most interesting and can be achieved by taking the deflection angle $70^\circ\,32'$ as can easily be seen from Eq. (2.10). In this case $D_3$ is $(2\sqrt{2})/3 = 0.943$, which is smaller than $6/\sqrt{34}$.

As the total ion path should be as short as possible, the length of $l_1$, $l_2$, $l_3$, and $d$ should be examined. Figs. 8 and 9 show that $l_1$ and $l_2$ become sufficiently short when $D_3$ approaches 1.0.

The length $l_3$ is a function of $\varphi_2$ and becomes short when $\varphi_2$ becomes large. Taking $D_3$ close to 1 and choosing $\varphi_2$ as large as possible the ion path from the source to the focal point becomes short.

According to Fig. 10, the instruments with $D_3 \simeq 1$ have a rather small ratio $r_{m0}/r_e$. This result seems favourable for a large instrument for mass determination, because a large electrostatic field is needed to increase its resolving power but a relatively small magnet meets the requirement. In the case of the smaller instruments such as those for solid analysis, however, a very small ratio $r_{m0}/r_e$ is of no practical use, as the effect of fringing field becomes serious. In this case the correction of the image defects for a particular mass, however, is not important but the reduction in defects for a wide mass range is essential. To fulfill this requirement, small $\overline{T}_{18}$ and $\overline{T}_{19}$ are needed. Figs. 12 and 13 show that these constants decrease with an increase in $D_3$ and $\varphi_2$.

All these conditions are fortunately compatible with each other.

The design parameters are numerically computed and tabulated in Table 1 for several favourable examples. Fig. 14 shows the configuration of typical examples.

Fig. 15 shows the change in the aberration coefficients along the focal plane as a function of $\tau$ for the mass spectrograph No. 4, Table 1. The change in these coefficients for the usual MATTAUCH–HERZOG

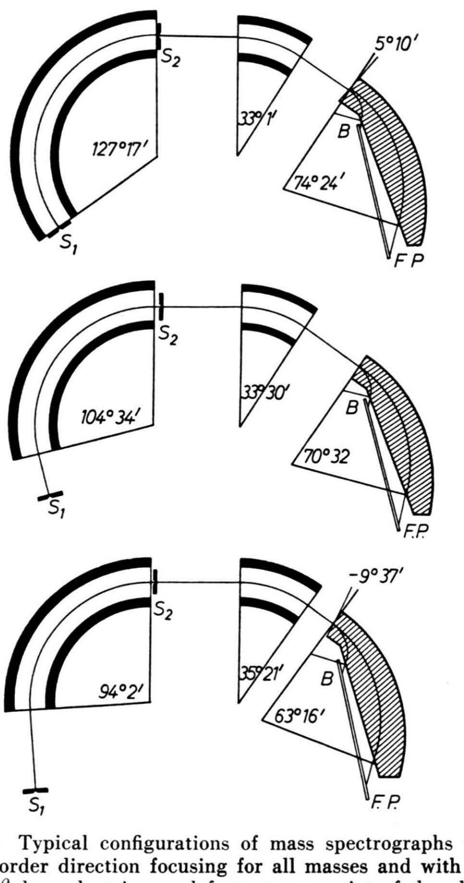


Fig. 14. Typical configurations of mass spectrographs with second-order direction focusing for all masses and with corrected $\beta$-dependent image defects at one point of the photoplate. $S_1$: Source slit, $S_2$: Energy slit, B: Second-order double focusing point, F.P.: Focal plane.

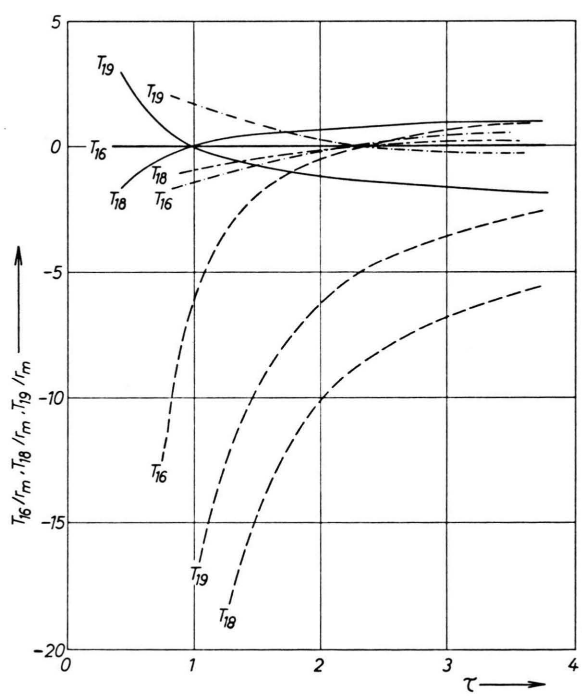


Fig. 15. Second-order aberration coefficients as a function of $\tau$ for mass spectrograph No. 4, Table 1. ——— TAKESHITA No. 4, Table 1; – – – – MATTAUCH ($d = r_e$); —·—·— HINTENBERGER [11] X−2.

type mass spectrograph and for HINTENBERGER's instrument X − 2 [11] are shown for comparison.

The total image defects due to the second-order aberration are the differences between the maximum and minimum values of $x$ given by Eq. (2.3) for any values of $\alpha$ and $\beta$ of the collected beams. In the present case, the area on the $\alpha-\beta$ plane defining the range of the permitted beam is rectangular, but in the usual case it becomes a parallelogram [12] as shown in Fig. 16 and its figure varies with the position of the energy slit.

Fig. 17 shows the total image defects of these three systems. Three curves are calculated under the following condition: The area of the rectangle and the parallelograms are equal ($\alpha_0=\beta_0=1$) that means, that the beam intensity is equal for each case. This figure shows that the image defects of the present instrument is considerably small. This fact results not only from the small coefficients of the second-order aberrations but also from the characteristic feature of this instrument, i. e. the independent control of the velocity spread and the beam divergence. The advantage of this instrument be-

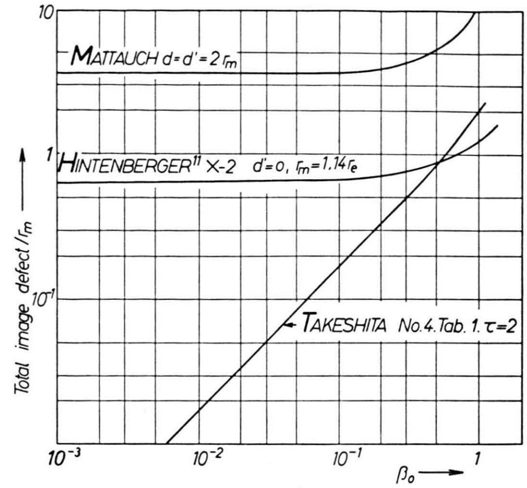


Fig. 18. Calculated total image defect as a function of $\beta_0$ ($\alpha_0$ is kept constant).

a) MATTAUCH–HERZOG type mass spectrograph with two-stage electrostatic field.

b) Usual MATTAUCH–HERZOG type mass spectrograph.

$$d=d'=r_e\,,\qquad \beta_0=\frac{W_S}{1.29\,r_e}\,.$$

c) HINTENBERGER [11] X−2

$$d'=0\,,\qquad \beta_0=\frac{W_S}{1.42\,r_e}\,,$$

$2\,W_S$: Width of energy slit.
$d$: Distance between electric field and magnetic field.
$d'$: Distance between electric field and energy slit.

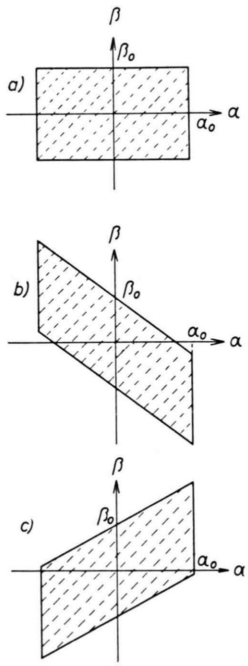


Fig. 16. Range of the permitted beam.

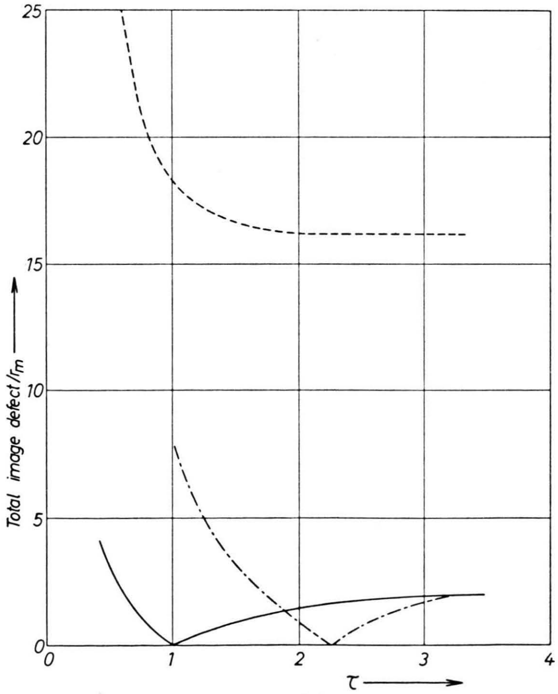


Fig. 17. Calculated total image defect as a function of $\tau$ for mass spectrograph No. 4, Table 1 ($\alpha_0=\beta_0=1$). ——— TAKESHITA No. 4, Table 1; – – – – MATTAUCH ($r_e=d=d'$); —·—·— HINTENBERGER [11] X−2 ($d'=0$).

[11] H. HINTENBERGER and L. A. KÖNIG, Advances in Mass Spectrometry (ed. J. D. WALDRON), Pergamon Press, London 1959, p. 34. X−2 is the abbreviation of No. 2 in Table X.

[12] I. TAKESHITA and K. MORIKAWA, Mass Spectroscopy (Japan) No. 16 [1960].

comes more clear when the change in the image defects are described as a function of $\beta_0$ under a constant value of $\alpha_0$.

Fig. 18 illustrates the results. Only by the present instrument the image defects can be decreased with decreasing $\beta_0$.

*Acknowledgement*

The author wishes to express his thanks to Professor K. OGATA and Professor H. MATSUDA for many helpful discussions and suggestions, to Dr. S. KISAKA, Manager of his Laboratory and Dr. C. OKAZAKI for their encouragement and to Mr. H. TANAKA for his programming of computer.

# A New Mass Spectrograph with Very Large Dispersion

H. MATSUDA, S. FUKUMOTO, and Y. KURODA

Institute of Physics, College of General Education, Osaka University

and M. NOJIRI

Japan Electron Optics Laboratory

(Z. Naturforschg. **21 a**, 25—33 [1966]; received 19 September 1965)

*Dedicated to Prof. J. MATTAUCH on his 70th birthday*

A new type of mass spectrograph with large mass dispersion has been constructed. The distinguishing feature of this apparatus is that the mass dispersing action of a $r^{-1}$ magnetic field is utilized. The instrument has a $r^{-1}$ magnetic field of 198.1° sector type (22 cm mean radius) as the dispersing field, a toroidal electric field of 118.7° sector type (30 cm mean radius) and a 30° uniform magnetic field (120 cm mean radius) as the focusing fields. The principle, the design and important parts of the apparatus are described. The dispersion on the photographic plate was estimated to be 14 cm for 1% mass difference and the maximum resolving power of about 500,000 was obtained.

A mass spectrograph with large mass dispersion and resolving power is useful for the precise determination of nuclidic masses. One method to obtain high resolution consists in enlarging the linear dimensions of the ordinary double focusing apparatus with cylindrical electric field and homogeneous magnetic field. During the past ten years, a number of large apparatus has been constructed [1], and a resolving power of several hundred thousand has been obtained. It seems, however, very difficult to enlarge the linear dimensions of the apparatus still more to increase the resolving power about one order of magnitude because of economic and technical reasons.

Another method for obtaining high resolution has been recently developed using a toroidal electric field and a non-uniform magnetic field [2]. Though this method is considered to be very promising, there might still be some technical difficulties in order to obtain a resolving power of several million.

About two years ago, one of the authors proposed a new method which might provide such high resolutions and mass dispersions without requiring very large linear dimensions [3]. It is the essential feature of this method to use a mass dispersing field which has no lens action. Since then, we were planning to construct a mass spectrograph which utilized this method. As a first step, in order to verify the principle experimentally and to study the characteristics of the dispersing field, we constructed a relatively small apparatus. The new mass spectrograph has a $r^{-1}$ magnetic field as the dispersing field together with a toroidal electric field and a uniform magnetic field as the focusing fields.

[1] K. OGATA and H. MATSUDA, Z. Naturforschg. **10 a, 843** [1955]. — K. S. QUISENBERRY, T. T. SCOLMAN, and A. O. NIER, Phys. Rev. **102,** 1071 [1956]. — C. STEVENS, J. TERANDY, G. LOBELL, J. WOLFE, N. BEYER, and R. LEWIS, Proc. Intern. Conf. Nuclidic Masses, University of Toronto Press, Toronto 1960, p. 403. — N. R. ISENOR, R. C. BARBER, and H. E. DUCKWORTH, ibid., p. 439. — K. T. BAINBRIDGE and P. E. MORELAND, JR., ibid., p. 460. — H. HINTENBERGER, J. MATTAUCH, H. WENDE, H. VOSHAGE, and W. MÜLLER-WARMUTH, Advan. Mass Spectr. **2,** 180 [1963]. — H. EWALD, E. KONECNY, H. OPOWER, and H. RÖSLER, Z. Naturforschg. **19 a,** 194 [1964].

[2] H. W. WACHSMUTH and H. EWALD, Z. Naturforschg. **18 a,** 389 [1963].

[3] H. MATSUDA, Mass Spectroscopy (Japan) **11,** 127 [1964].